


ActiveNeuS: Active 3D Reconstruction using Neural Implicit Surface Uncertainty

Hyunseo Kim¹ , Hyeonseo Yang¹, Taekyung Kim², YoonSung Kim¹,
Jin-Hwa Kim^{*2,3}, and Byoung-Tak Zhang^{*1,3}

¹ Seoul National University

² NAVER AI Lab

³ AIIS

{hskim, hsyang, yskim, btzhang}@bi.snu.ac.kr
{jlnhwa.kim, taekyung.k}@navercorp.com

Abstract. Active learning in 3D scene reconstruction has been widely studied, as selecting informative training views is critical for the reconstruction. Recently, Neural Radiance Fields (NeRF) variants have shown performance increases in active 3D reconstruction using image rendering or geometric uncertainty. However, the simultaneous consideration of both uncertainties in selecting informative views remains unexplored, while utilizing different types of uncertainty can reduce the bias that arises in the early training stage with sparse inputs. In this paper, we propose ActiveNeuS, which evaluates candidate views considering both uncertainties. ActiveNeuS provides a way to accumulate image rendering uncertainty while avoiding the bias that the estimated densities can introduce. ActiveNeuS computes the *neural implicit surface uncertainty*, providing the color uncertainty along with the surface information. It efficiently handles the bias by using the surface information and a grid, enabling the fast selection of diverse viewpoints. Our method outperforms previous works on popular datasets, Blender and DTU, showing that the views selected by ActiveNeuS significantly improve performance.

Keywords: active learning · neural implicit surface uncertainty · surface grid

1 Introduction

Active learning in 3D reconstruction has been widely studied to deal with the difficulties in multi-view data collection [1]. Recent advances in neural networks for 3D reconstruction show that 3D scenes can be represented using implicit neural representations (INR) with higher output quality and smaller space usage. However, popular approaches such as Neural Radiance Fields (NeRF) [16] require a large number of multi-view posed images for effective generalization of neural networks [26]. To alleviate the data collection burden, active learning of INR emerged and provided a way to select the most informative data samples for training.

Estimating uncertainty is one of the popular methods to measure informativeness in active learning [5, 18, 24]. Active learning in NeRF typically estimates the uncertainties in its outputs: density and color of 3D points. Martin *et al.* [15] and Pan *et al.* [18] estimated uncertainties in color prediction by modeling the color as a Gaussian probability

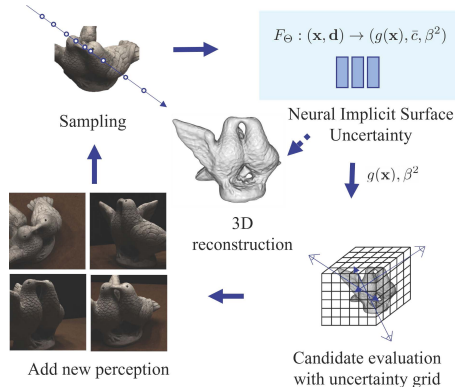


Fig. 1: ActiveNeuS Framework. First, we sample 3D points in the given views. Using the points, a neural implicit surface network is trained to predict the points’ SDF $g(\mathbf{x})$ and color uncertainty β^2 . The surface information computed from the SDF and the uncertainty are stored in the surface and uncertainty grids, respectively. We choose the next-best views among candidates using both grids. After adding new perceptions, we continue the sampling process again.

distribution and using its variance to measure uncertainty. On the other hand, Zhan *et al.* [29] and Lee *et al.* [13] measured the entropy of density-related information (*e.g.* occupancy probabilities and weight) concerning the scene geometry.

However, as shown in Fig. 2, active 3D reconstruction methods considering only one type of uncertainty, color or density, insufficiently provide information about the other. The lack of information may introduce the bias in uncertainty integration. ActiveNeRF [18] evaluated the informativeness of candidate views as the difference in color variance between a 3D point’s prior distribution and its predicted posterior distribution after a candidate view is incorporated. As shown in the right column of Fig. 2b, the difference in color variance does not reflect the geometric characteristic of the scene. Entropy method [3, 29] shown in Fig. 2c, exhibits geometric property in its acquisition value. Still, it may not convey useful information at the early training stage when the density information has not converged yet. Moreover, the occupancy probabilities lack information about the color prediction’s quality, making it fail to provide useful information for image rendering [9].

For a successful combination of image rendering and geometric uncertainties, we present ActiveNeuS, the active 3D reconstruction framework using neural implicit surface uncertainty (Fig. 1). We introduce the neural implicit surface uncertainty, the color uncertainty newly defined in the neural implicit surface framework [23]. As shown in Fig. 1, we calculate the information gain of candidate views using the surface and uncertainty grid and refine the reconstruction with the newly incorporated views. We evaluate the efficacy of our proposed framework on the Blender and DTU datasets. Our method outperforms other methods in image rendering and mesh reconstruction qualitatively and quantitatively. We show ActiveNeuS selects diverse viewpoints that lead to performance improvement, and we conduct ablation studies to show the significance of surface information in our method.

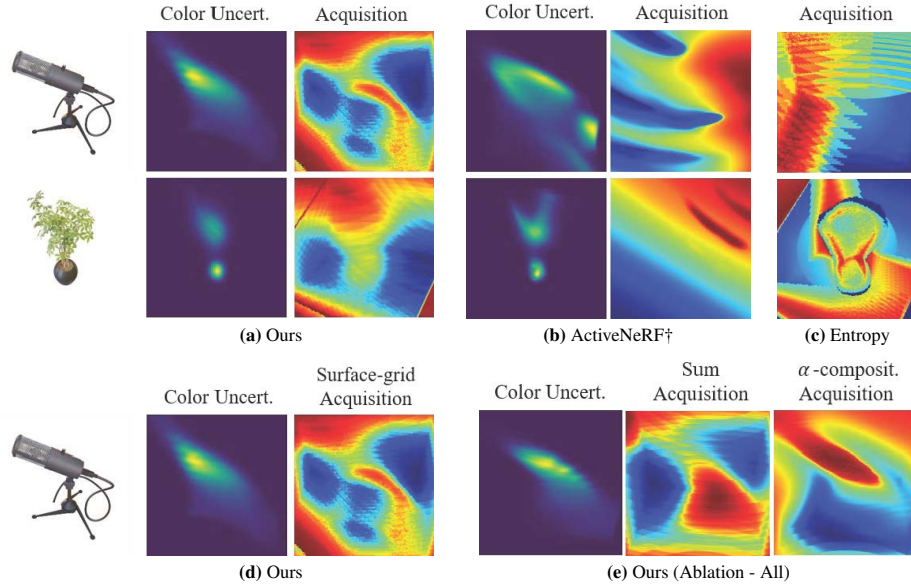


Fig. 2: Pixel-wise acquisition values and corresponding uncertainty of methods are visualized. The images taken from a mic scene are captured when the training is 5% progressed (5 views collected), and those of ficus are captured at 3% of the training process (3 views collected). Entropy method does not calculate uncertainty explicitly and utilizes occupancy probabilities for the acquisition calculation. Thus, only the acquisition value is presented. Also, all color uncertainties in this figure are calculated in the same way. ActiveNeRF \dagger is ActiveNeRF implemented in the neural implicit surface framework and has the same point sampling strategy as ours. (Acquisition: blue for low value and red for high value, color uncertainty: blue for low and yellow for high)

Motivation. Inspired by Entropy method [13, 29], we calculate color entropy from the color uncertainty to use it as an information gain that preserves geometric information. However, simply summing up the color entropy like in the entropy method would lead to an inaccurate integration caused by incorporating the color entropy behind surfaces (the middle image in Fig. 2e). Some of the density estimation of the cord part under the microphone has not converged yet, and the others have converged to a surface in the early training stage. The lump of incompletely reconstructed and low-density points occurs, resulting in high entropy in that area under the summation method.

Also, using the α -composition [19] technique as in NeRF variants [16, 18] to indirectly infer the surface can result in biased estimation (the right side image in Fig. 2e). The α -composition accumulates the weighted color uncertainties of 3D points along camera rays, reducing the influence rates of the low-density points' color entropy in the final acquisition value. As shown on the right image of Fig. 2e, the color entropy of the cord part under the microphone is ignored, and the color entropy on the head of the microphone is magnified.

To successfully integrate color entropy, the entropy should originate from the reducible color uncertainty located on the surface or in the cloud of incomplete recon-

struction. The explicit definition of the surface makes the filtering of color entropy possible. The use of explicit surface information prevents the color entropy from being biased by the density distribution during integration. Fig. 2d shows the integrated color entropy using surface information well reflects the expected information gain.

Contributions. In summary, the contributions of the paper are as follows: (1) We propose a new acquisition function considering geometric and image reconstruction fidelity. Our method suggests integrating color entropy without being exposed to the bias that the density information may introduce during integration. (2) We propose a neural implicit surface uncertainty that works as a color uncertainty under a neural implicit surface network. The surface information and the color uncertainty are earned while computing the neural implicit surface uncertainty. (3) We present a surface and an uncertainty grid that efficiently integrate the color entropy using surface information.

2 Related Work

2.1 Uncertainty in Active 3D Reconstruction

Prior works in active 3D reconstruction that emphasized geometric fidelity measured uncertainty in volumetric representations such as voxels or meshes [3, 7]. For example, in active robotics 3D reconstruction, the degree of observability is often regarded as uncertainty [7]. When the robot observes a specific part, the occupancy probability approaches 0 or 1, resulting in lower entropy and reduced uncertainty. However, the reliance on volumetric representation often limits the quality of the rendered output, as it relies heavily on the resolution of grid cells.

The SDF field is not constrained by resolution limitations, so it has been used for 3D reconstruction as one of the alternatives. A lot of works adopted the Gaussian distribution to model uncertainty in SDF-based reconstructions [4, 21]. However, they focused on modeling the geometric uncertainty rather than color.

2.2 Active 3D Reconstruction using Neural Implicit Representation

As neural implicit representations are increasingly applied in the active reconstruction field, various forms of uncertainty are utilized for NBV selections [9, 13, 18, 20, 29]. There are works that measure geometric uncertainty using the entropy of sample points' weights along a ray [13] and the entropy of occupancy probability throughout the scene [29], following the traditional geometric uncertainty estimation methods. These approaches focused on improving the outputs' geometric fidelity rather than the image rendering quality [13, 29]. While ActiveRMAP [29] evaluated the image rendering quality of its outputs, it does not directly consider image rendering quality in the NBV selection, which indicates color prediction performance solely depends on the base framework's performance. Additionally, Lee *et al.* [13] requires initialization with camera views from a 360-degree perspective, making it challenging to apply in common scenarios.

On the other hand, there are works that measure uncertainty in color, primarily modeling it as a Gaussian probability distribution. They mainly focused on improving the image rendering quality rather than geometric fidelity [9, 18, 20]. NeurAR [20]

evaluated geometric fidelity in its outputs, but it was achievable as it utilized depth information during training. Meanwhile, NeU-NBV [9] concentrates on more accurate color uncertainty estimation to optimize planning trajectories. NBV planning or optimization papers calculate an information gain with their proposed policies, not in the form of an acquisition function. Therefore, we do not compare our method with NBV planning methods in this paper. Throughout the paper, we compare our method to ActiveNeRF [18] and demonstrate the simultaneous consideration of geometric and image rendering fidelity generally diversifies the NBV selection and improves performance in both criteria.

3 Preliminaries

In this section, we will briefly review the Neural Radiance Field (NeRF) [16] and NeuS [23], and introduce basic concepts for further discussion, including the uncertainty estimation in NeRF as a background of our work.

3.1 Neural Implicit Representations

NeRF [16] represents a 3D scene as a continuous function, denoted as $F_{\Theta} : (\mathbf{x}, \mathbf{d}) \rightarrow (\sigma, \mathbf{c})$. This function takes a 3D point’s position $\mathbf{x} = (x, y, z)$ and a viewing direction $\mathbf{d} = (d_x, d_y, d_z)$, and outputs the density σ and color radiance $\mathbf{c} = (r, g, b)$. NeRF studies the relationship between inputs and outputs through classical volume rendering [10]. Specifically, it accumulates information from sample points on the ray $\mathbf{r}(t) = \mathbf{o} + t\mathbf{d}$ where the camera center \mathbf{o} and the view direction \mathbf{d} are given. The resulting color of the ray is calculated as follows:

$$C(\mathbf{r}) = \int_{t_n}^{t_f} T(t)\sigma(\mathbf{r}(t))\mathbf{c}(\mathbf{r}(t), \mathbf{d})dt, \quad \text{where } T(t) = \exp\left(-\int_{t_n}^t \sigma(\mathbf{r}(s))ds\right) \quad (1)$$

The integration of color value along the ray occurs from the near plane t_n to the far plane t_f . NeRF employs stratified sampling with N points sampled along the ray to make the rendering process tractable. The quadrature of the color rendering using the stratified sampling is formulated as follows:

$$\hat{C}(\mathbf{r}) = \sum_{i=1}^N T_i\alpha_i\mathbf{c}_i, \quad \text{where } T_i = \prod_{j=1}^{i-1}(1 - \alpha_j), \quad \alpha_i = 1 - \exp(-\sigma_i\delta_i) \quad (2)$$

where the distance between adjacent samples is $\delta_i = t_{i+1} - t_i$. NeRF is trained with the mean squared error (MSE) loss between the ground truth color and the rendered color. However, it has limitations in the precise inference of surfaces from learned neural implicit representation due to the absence of adequate surface constraints. Moreover, near-surface noises may persist even after training completion. These noises are typically observed within a limited range of ray directions, as these are easily occluded by the surface, especially if the surface is concave. If the information from various viewpoints is insufficient, the sampled points near surfaces may appear as objects with varying colors depending on the direction.

NeuS [23] utilizes a neural signed distance function (SDF) in the volume rendering. The NeuS’s network $F_\Theta : (\mathbf{x}, \mathbf{d}) \rightarrow (g(\mathbf{x}), \mathbf{c})$ is similar to NeRF, but the key difference is the SDF $g(\mathbf{x})$ instead of density σ . The SDF’s zero-level set represents an object’s surface \mathcal{S} :

$$\mathcal{S} = \{\mathbf{x} \in \mathbb{R}^3 | g(\mathbf{x}) = 0\}. \quad (3)$$

NeuS introduces the S-density field $\phi_s(g(\mathbf{x}))$ to integrate the SDF in the volume rendering. The $\phi_s(g(\mathbf{x}))$ denotes the derivative of the Sigmoid function $\Phi_s(x) = (1 + e^{-sx})^{-1}$, a zero-centered unimodal density distribution. Note that the standard deviation of ϕ_s is $1/s$, which approaches zero as training converges with a learnable parameter s . The value $1/s$ is also interpreted as the point sampling step size, which means the network infers a more precise and thinner surface as training progresses. To deal with general cases, NeuS introduces opaque density ρ , analogous to NeRF’s volume density σ , which leads to the definition of different α values but allows similar usage of Eq. (2):

$$\alpha_i = 1 - \exp\left(-\int_{t_i}^{t_{i+1}} \rho(t) dt\right), \quad \rho(t) = \max\left(\frac{-\frac{d\Phi_s}{dt}(g(\mathbf{r}(t)))}{\Phi_s(g(\mathbf{r}(t)))}, 0\right) \quad (4)$$

Then, α is determined by the quadrature using the stratified sampling of N points along a ray.

$$\alpha_i = \max\left(\frac{\Phi_s(g(\mathbf{r}(t_i))) - \Phi_s(g(\mathbf{r}(t_{i+1})))}{\Phi_s(g(\mathbf{r}(t_i)))}, 0\right) \quad (5)$$

The final loss function consists of color and eikonal [6] regularization losses. The color loss is summed up for M rays, where $C(\mathbf{r})$ and $\hat{C}(\mathbf{r})$ are the ground truth and the predicted colors for the ray \mathbf{r} , respectively. The eikonal loss encourages the gradients $\nabla g(\mathbf{r}_i(t_j))$ to be of unit 2-norm, and with a parameter λ , the average is taken to the number of sample points N and rays M .

$$\mathcal{L}_s = \frac{1}{M} \sum_{i=1}^M \left[\|\hat{C}(\mathbf{r}_i) - C(\mathbf{r}_i)\|_1 + \frac{\lambda}{N} \sum_{j=1}^N (\|\nabla g(\mathbf{r}_i(t_j))\|_2 - 1)^2 \right] \quad (6)$$

3.2 Uncertainty in Neural Radiance Field

Active learning to incrementally select the next-best view requires the estimation of ray uncertainty. ActiveNeRF [18] and other works [12, 15] modeled the color value at each 3D location with a Gaussian distribution rather than a single value. By doing so, the ray uncertainty is calculated using the color variances for the samples on the ray. The network structure of ActiveNeRF is defined as: $F_\Theta : (\mathbf{x}, \mathbf{d}) \rightarrow (\bar{c}, \beta^2, \sigma)$, where \bar{c} and β^2 represent the mean and variance of the color c , respectively.

$$c(\mathbf{r}(t)) \sim \mathcal{N}(\bar{c}(\mathbf{r}(t)), \beta^2(\mathbf{r}(t))) \quad (7)$$

The mean and variance of a ray are rendered through the volume rendering in Eq. (2).

$$\bar{C}(\mathbf{r}) = \sum_{i=1}^N T_i \alpha_i \bar{c}(\mathbf{r}(t_i)), \quad \mathcal{B}^2(\mathbf{r}) = \sum_{i=1}^N T_i^2 \alpha_i^2 \beta^2(\mathbf{r}(t_i)) \quad (8)$$

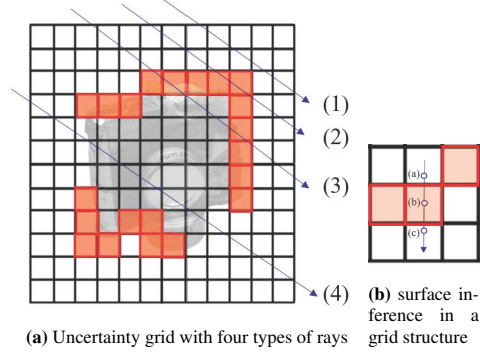


Fig. 3: Example of the uncertainty grid coupled with surface information. The grids shadowed in red represent inferred surfaces. **(a):** (1) and (4) indicate a case in which a ray passes through uncertainty grids that do not contain inferred surface grids. (2) and (3) indicate a case in which a ray passes through the surface once or more. **(b):** It demonstrates how we infer the surface from the surface grid. The center point (b) of a grid cell is sampled with random noise, and points (a) and (c) are on the same ray as (b). The distance between (a) and (c) is the step size $1/s$, and (b) is the middle point. Since the surface is the zero-level set of SDF (Eq. (3)), the multiplication of the SDF values of (a) and (c) should be negative. The estimation of surface converges as training progresses, and the step size decreases.

Then, the resulting ray color follows a Gaussian distribution defined as:

$$\hat{C}(\mathbf{r}) \sim \mathcal{N}(\bar{C}(\mathbf{r}), \mathcal{B}^2(\mathbf{r})). \quad (9)$$

Finally, the negative log-likelihood of the probability distribution of $\hat{C}(\mathbf{r})$ is incorporated as the uncertainty loss \mathcal{L}_u to optimize the mean and variance of a ray defined as follows [18]:

$$\mathcal{L}_u = \frac{1}{M} \sum_{i=1}^M \left(\frac{\|\bar{C}(\mathbf{r}_i) - C(\mathbf{r}_i)\|_2^2}{2\mathcal{B}^2(\mathbf{r}_i)} + \frac{\log \mathcal{B}^2(\mathbf{r}_i)}{2} \right) \quad (10)$$

where $C(\mathbf{r}_i)$ is the ground truth color from a training image.

ActiveNeRF calculates the information gain of a camera view v as the reduction in variance caused by the influence from the camera view v , defined as follows:

$$\mathcal{A}(v) = \sum_{\forall \mathbf{r} \in \mathcal{R}_v} \sum_{j=1}^N \left[\beta^2(\mathbf{r}(t_j)) - \left(\frac{1}{\beta^2(\mathbf{r}(t_j)) + \frac{T_j^2 \alpha_j^2}{\mathcal{B}^2(\mathbf{r})}} \right)^{-1} \right] \quad (11)$$

where the first term is the variance of the prior distribution and the second term is the variance of the posterior distribution. As mentioned in Sec. 1, the difference in variance between the prior distribution and the posterior distribution does not contain the geometric property of a scene in the early training stage. Therefore, the acquisition function of ActiveNeRF (Eq. (11)) does not manifest geometric property.

4 Method

In this section, we propose a new acquisition function incorporating geometric reconstruction and image rendering perspectives. Our model, ActiveNeuS, estimates uncertainty regarding color prediction to obtain information about image rendering quality. Our acquisition function integrates the estimated uncertainty without losing geometric property. First, in Sec. 4.1, we introduce our acquisition function and explain how to consider a surface during the integration process. In Sec. 4.2, we define the neural implicit surface uncertainty, estimated in ActiveNeuS, and describe how the uncertainty is utilized in our acquisition function. Then, for efficient and robust computation, we introduce a surface grid that stores the surface information and a strategy to select multiple next-best views (NBVs) (Sec. 4.3).

4.1 Acquisition Function using Surface

Inspired by Entropy methods that consider geometric uncertainty, our acquisition function is implemented using the grid structure, enabling efficient and robust calculation. We also utilize the method to integrate the grids’ information, which originally uses an occupancy grid [7]. First, we measure the information of the grid cells to compute the information gain. The information of the occupancy grid map, for example, is defined as the entropy $I(x)$ of grid cells x [7]. Similarly, we define the uncertainty grid as a grid that stores ActiveNeuS’s uncertainty and designate the information of the uncertainty grid as the color entropy $H(c)$. The definition of color entropy will be introduced in Sec. 4.2. $I(x)$ is formulated as:

$$I(x) = -p(x) \log p(x) - (1 - p(x)) \log(1 - p(x)). \quad (12)$$

To make the entropy $I(x)$ highest when the grid is initialized, the occupancy probability $p(x)$ of the occupancy grid map is initialized in 0.5. In this paper, we define $p(x)$ as α in Eq. (4) when implementing the entropy method with the neural implicit surface representation.

The information gain of a camera view is defined as the sum of information inside the camera frustum [22]. Let \mathcal{R}_v be the set of rays cast through the sampled points on camera view v , and \mathcal{X} be the set of occupancy grid cells that the rays traverse through. When n is the total number of traversed grid cells, the information gain $G(v)$ of a camera view v is defined as:

$$G(v) = \frac{1}{n} \sum_{\forall r \in \mathcal{R}_v} \sum_{\forall x \in \mathcal{X}_r} I(x). \quad (13)$$

However, the naive summation of color entropy $H(c)$ like in Eq. (13) results in the inaccurate computation of information gain due to the bias introduced by the density as described in Sec. 1. Therefore, we consider the surface information that corresponds with the uncertainty grid.

We define a surface grid as a grid that stores the probability of being a surface. The detailed definition is stated in Sec. 4.3. We define the set of surface grid cells \mathcal{S} with the grid cells that have surface grid values above a parameterized threshold. As depicted

in Fig. 3a, the integration method of color entropy from the uncertainty grid differs by the presence of the surface. When \mathcal{S} is an empty set, indicating that the ray r does not intersect the surface, we aggregate the entire color entropy $H(c)$ from the uncertainty grids traversed by the ray. When \mathcal{S} is not an empty set, we consider the color entropy $H(c)$ only from the cell in \mathcal{S} . Here, n represents the number of uncertainty grid cells that constitute the surface when \mathcal{S} is not an empty set, and if it is, n represents the number of uncertainty grid cells that the ray traverses.

$$G_s(v) = \frac{1}{n} \sum_{\forall r \in \mathcal{R}_v} \sum_{\forall x \in \mathcal{X}_r \cap \mathcal{S}} H(c(x)) \quad (14)$$

Our acquisition function $G_s(v)$ indirectly reflects geometric uncertainties by integrating all color uncertainties in a ray that traverses incomplete surface reconstruction. When a ray traverses a surface, $G_s(v)$ considers only the color uncertainty on a surface, conveying relatively low uncertainty compared to the uncertainty in an incomplete reconstruction part.

4.2 Estimation of Surface and Color Entropy

ActiveNeuS represents the color of a 3D point as a Gaussian probability distribution to measure the image reconstruction uncertainty. Given a 3D point’s position \mathbf{x} and a viewing direction \mathbf{d} , ActiveNeuS estimates the SDF $g(\mathbf{x})$, and the mean \bar{c} and variance β^2 of the color, denoted as $F_\Theta : (\mathbf{x}, \mathbf{d}) \rightarrow (g(\mathbf{x}), \bar{c}, \beta^2)$. We define the color variance β^2 as the neural implicit surface uncertainty, which measures the confidence of color estimation. Notice that α defined in NeuS (Eq. (4)) is different from α defined in NeRF (Eq. (2)) when calculating the ray color and the color uncertainty of a ray in Eq. (8).

The uncertainty loss function \mathcal{L}_u defined in Eq. (10) is incorporated in the loss function \mathcal{L} with a parameter ω to estimate the color while reducing the variance. For the surface, the loss function \mathcal{L} includes \mathcal{L}_s (Eq. (6)) from NeuS framework.

$$\mathcal{L} = \mathcal{L}_s + \omega \mathcal{L}_u \quad (15)$$

Based on the definition of an uncertainty grid in Sec. 4.1, the neural implicit surface uncertainty β^2 is stored in the uncertainty grid using a growth rate 1.05. We adopt the growth rate to store the view-dependent color uncertainty in the uncertainty grid for efficient computation. Empirically, the value of color uncertainty does not change abruptly according to the viewpoint in convex objects. Also, as we integrate color entropy from multiple 3D points to calculate an information gain, minor inaccuracies in color uncertainty can be ignored. For objects that have concave surfaces, only a subset of viewpoints can provide accurate information about the points on the concave surfaces, and other viewpoints would have difficulty in reducing the uncertainty on the points. Therefore, for efficient computation, the uncertainty grid stores the minimum of the predicted uncertainties with a growth rate of 1.05, similar to the occupancy grid update [17] but in the opposite way.

Table 1: Quantitative comparison on Blender. Image rendering qualities are evaluated using PSNR, SSIM, and LPIPS scores. ActiveNeRF \dagger differs from ActiveNeRF in that it uses accelerated grid sampling [14, 17] for more efficient training. ActiveNeRF \dagger uses the same sampling strategy with ActiveNeRF in the view selecting stage. A total of 5, 10, and 20 images are used in training in 1, 2, and 4-image settings, respectively.

		1-image setting			2-image setting			4-image setting		
Methods		PSNR \uparrow	SSIM \uparrow	LPIPS \downarrow	PSNR \uparrow	SSIM \uparrow	LPIPS \downarrow	PSNR \uparrow	SSIM \uparrow	LPIPS \downarrow
density	Random	11.05	0.744	0.442	12.34	0.759	0.404	26.68	0.909	0.089
	Entropy	11.45	0.752	0.423	12.70	0.779	0.383	25.71	0.899	0.100
	ActiveNeRF \dagger	13.09	0.776	0.362	16.64	0.807	0.270	18.82	0.822	0.261
	ActiveNeRF [18]	-	-	-	20.01	0.832	0.204	26.24	0.856	0.124
	ActiveNeRF (repro.)	-	-	-	14.78	0.792	0.251	17.00	0.820	0.200
surface	Random	15.88	0.812	0.268	16.24	0.831	0.268	21.79	0.874	0.151
	Entropy	13.78	0.801	0.307	15.41	0.818	0.291	21.28	0.869	0.159
	ActiveNeRF \dagger	15.93	0.809	0.270	19.25	0.841	0.208	23.91	0.884	0.127
	Ours	16.63	0.809	0.265	21.22	0.854	0.170	26.08	0.907	0.106

As we define the color as a Gaussian probability distribution, the entropy H of the color is defined with the variance β^2 of the color [2], as follows:

$$H(c(\mathbf{r}(t))) = -\mathbb{E}[\log \mathcal{N}(\bar{c}(\mathbf{r}(t)), \beta^2(\mathbf{r}(t)))] \quad (16)$$

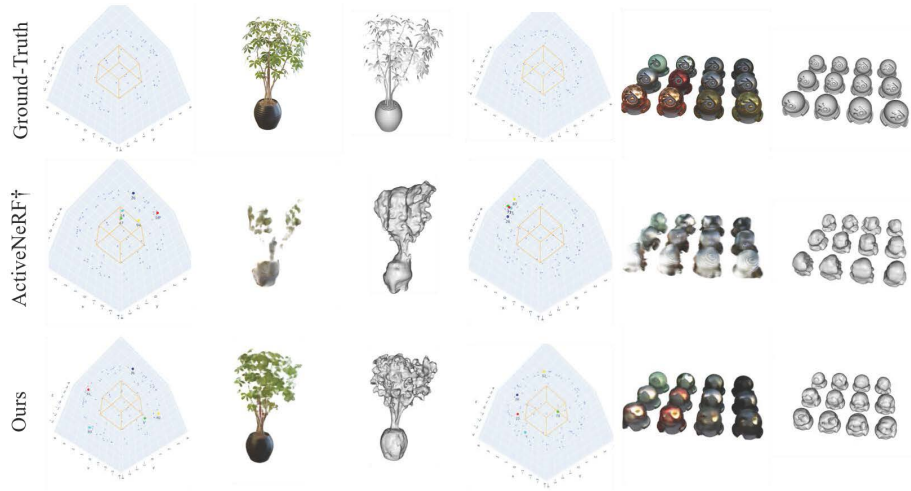
$$= \frac{1}{2} \log(2\pi\beta^2) + \frac{1}{2} \quad (17)$$

Empirically, the neural implicit surface uncertainty has values in the range of 0 to 1, so we set the initial value of the uncertainty grid as 1 to make the entropy highest. Therefore, we can estimate the information in the uncertainty grid as a color entropy like the Entropy method.

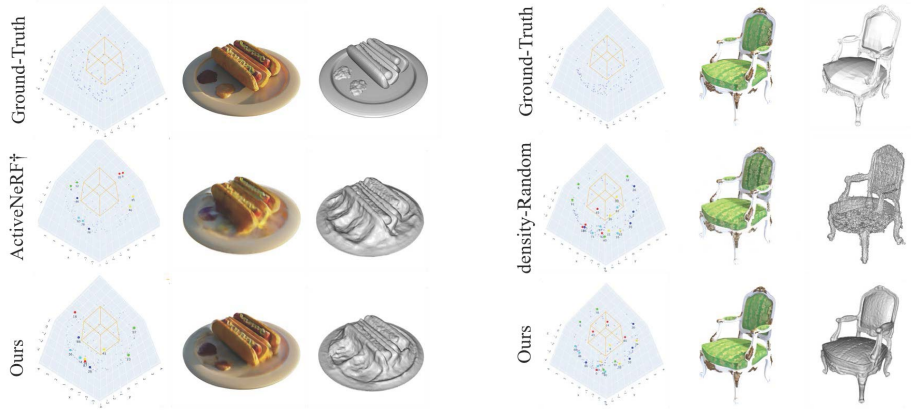
4.3 Surface Grid and Selection Strategy

ActiveNeuS estimates the SDF $g(\mathbf{x})$, and the property of SDF states that 3D points outside a surface have a positive SDF value, while insiders have a negative SDF value. Therefore, if two adjacent sampled points have different sign values in the SDF, we can infer that the surface exists between them. We defined the surface grid as a grid that stores surface information. We can sample 3D points in the surface grid cells and evaluate their probability of being surfaces. In Fig. 3b, we illustrate how we infer the surface grid cell. When the points (a) and (c) have different sign values in the SDF, the surface grid value of (b) is updated to 1. If the two points have the same sign values, the surface grid is updated to 0. Despite the randomness in point (b) position, the surface status does not change abruptly using a decay rate and a suitable parameterized threshold.

Multiple next-best view selection Selecting multiple NBVs becomes essential when acquiring diverse perspectives within limited computational resources and time constraints. Without additional criteria, simply choosing the top k candidates based on the acquisition value can lead to the selection of similar views from specific regions of the



(a) results in a 1-image setting on Blender. (Ours and surface-ActiveNeRF†)



(b) results in a 2-image setting on Blender. (Ours and surface-ActiveNeRF†)

(c) results in a 4-image setting on Blender. (Ours and density-Random)

Fig. 4: Ground-Truth and the best-performing algorithms are compared. The visualization of camera coordinates of selected train images, rendered RGB images, and reconstructed meshes are shown from left to right. The inputs are chosen in the order of blue-cyan-green-yellow-red. Our selection of camera views exhibits more diversity, covering top and 360-degree views, resulting in more accurate rendering and meshes.

camera sphere. This redundancy may limit the diversity of information. To address this issue, we introduce a strategy to ensure that the selected k images are sufficiently spaced apart. Algorithm 1 in Appendix outlines the procedure for selecting these k candidates.

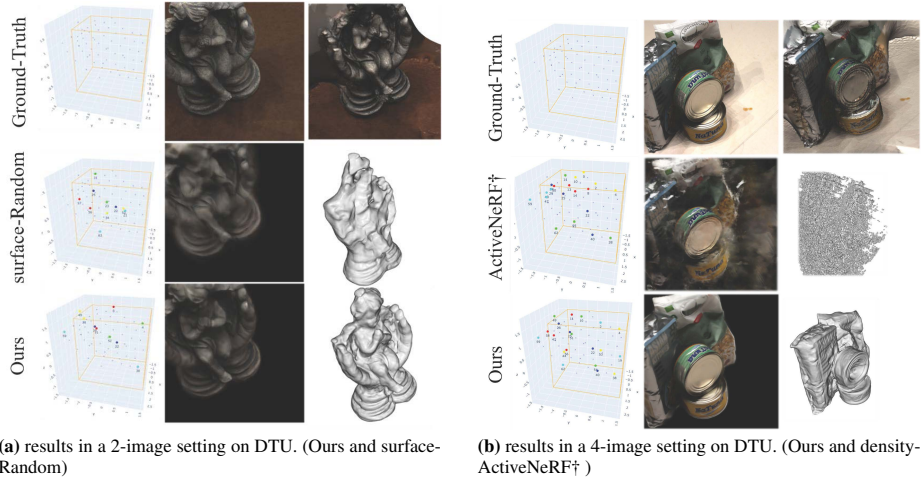


Fig. 5: Ground-Truth and the best-performing algorithms are compared. The visualization of camera coordinates of selected train images, rendered RGB images, and reconstructed meshes are shown from left to right. The camera inputs are chosen in the order of blue-cyan-green-yellow-red. Our camera pose selection covers a wider range of XYZ coordinates, resulting in more accurate rendering and meshes.

Table 2: Quantitative comparison on DTU. Image rendering qualities are evaluated using PSNR, SSIM, and LPIPS scores. Mesh completeness is evaluated using accuracy, completeness, and chamfer distance. A total of 10 and 20 images are used in training in 2 and 4-image settings, respectively.

		2-image setting						4-image setting					
Methods		PSNR \uparrow	SSIM \uparrow	LPIPS \downarrow	Acc. \downarrow	Comp. \downarrow	Chamfer \downarrow	PSNR \uparrow	SSIM \uparrow	LPIPS \downarrow	Acc. \downarrow	Comp. \downarrow	Chamfer \downarrow
density	Random	21.17	0.769	0.238	5.166	8.680	6.923	28.14	0.896	0.101	5.084	5.757	5.420
	Entropy	16.86	0.684	0.299	4.760	6.886	5.823	26.09	0.866	0.127	5.230	5.580	5.405
	ActiveNeRF†	21.78	0.786	0.229	5.862	9.955	7.909	29.56	0.911	0.090	6.345	8.269	7.307
surface	Random	27.69	0.864	0.170	2.368	3.472	2.920	29.34	0.907	0.111	1.765	2.340	2.053
	Entropy	24.21	0.810	0.218	2.861	4.426	3.644	27.36	0.872	0.147	2.206	3.198	2.702
	ActiveNeRF†	26.30	0.852	0.175	2.026	2.763	2.395	28.25	0.873	0.137	2.702	2.182	2.021
	Ours	28.19	0.867	0.168	1.829	2.176	2.002	30.10	0.910	0.116	1.715	1.967	1.864

5 Experiment

5.1 Experimental Setup

Datasets. We evaluate our method on two datasets using active learning schemes: 15 scenes from the DTU dataset [8] and 8 scenes from the NeRF Blender Synthetic dataset (Blender) [16]. For DTU, each scene contains 49 or 64 images, and 10 images are reserved for the test. For Blender, each scene contains 100 train images and 200 test images, but we used 25 evenly sampled images for the test.

Active learning scheme. We evaluate the reconstruction performance mainly in two settings: 2-image and 4-image settings, and we additionally implemented a 1-image

setting in the Blender dataset. During training, the model selects the next-best view images with the prespecified iteration interval four times. We set the iteration interval as $0.5k$, $1k$, $2k$ in 1-image, 2-image, and 4-image settings, respectively. Therefore, a total of 5, 10, and 20 images are used in training in 1, 2, and 4-image settings, respectively. Detailed experiment settings are described in Appendix Sec. 7.2.

Comparing methods. We test our method against two types of next-best view (NBV) acquisition methods: Entropy and ActiveNeRF \dagger . The entropy method selects NBV with the highest entropy sum of occupancy probabilities (Eq. (13)). ActiveNeRF \dagger method selects a view that reduces the color variance the most (Eq. (11)). We also implemented the methods in two types of representations: density and surface. Since the entropy [3,29] and ActiveNeRF [18] were originally developed in the density representation, we implemented them with both representations; density, to compare with the original implementation, and surface, for a fair comparison with ours. ActiveNeRF \dagger in surface representation shares the model architecture with our method and only differs in the NBV selection method, which makes it a more fair comparison. We also compared our method to ActiveNeRF with its official code, but we could not reproduce the results reported in the paper. Further details are described in Appendix Sec. 7.1.

5.2 Comparison

Blender dataset. We evaluated the effectiveness of image selection on image rendering quality (Tab. 1) and mesh reconstruction quality. In the 1-image and 2-image settings, our method shows outstanding results in both criteria as images from diverse viewpoints are selected (Fig. 4a and Fig. 4b). The result of ActiveNeRF \dagger shows that some parts of objects are colored white, which occurs when the model does not have enough color information on those parts because of the lack of diverse viewpoints. In the 4-image setting, as the total number of train images is large enough for the random selection to cover the hemisphere, *the benefit of effective image selection is reduced* (Fig. 4c).

Time comparison. We compared the time to select the next-best views (NBV) in the 2-image setting in Blender. The NBV selection times are averaged over eight scenes (Fig. 6). Our method (0.8 s) has significantly improved time consumption compared to ActiveNeRF \dagger (10 s) and has a similar time consumption to Entropy (0.5 s).

DTU dataset. Our method outperforms other next-best view selection methods both in mesh reconstruction and image rendering, quantitatively (Tab. 2) and qualitatively. As shown in Fig. 5, random selection can cover a wide viewpoint range but cannot focus on incompletely reconstructed parts. Also, ActiveNeRF \dagger with density representation performs well in image rendering but not in mesh reconstruction. We trained all methods with object masks applied to the DTU dataset for a fair evaluation. If we evaluate methods on DTU without masks, surface-based methods should handle the uncertainties from two different networks (NeRF and NeuS) because the surface-based methods additionally need a background model (*e.g.*, NeRF) for background training [23].

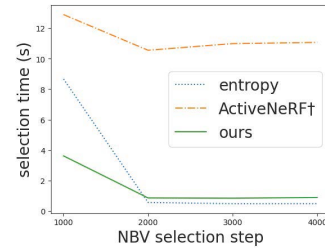


Fig. 6: NBV select. time

Table 3: Ablation studies on ActiveNeuS selection strategy. Strategies are evaluated in a 2-image setting. ‘Top’ denotes that the strategy selects k views with high acquisition values without further criteria. ‘All’ denotes that the estimated uncertainties are integrated without considering surfaces: $\forall x \in \mathcal{X}_r$ in Eq. (14).

		Blender			DTU						
		K	PSNR \uparrow	SSIM \uparrow	LPIPS \downarrow	PSNR \uparrow	SSIM \uparrow	LPIPS \downarrow	Acc. \downarrow	Comp. \downarrow	Chamfer \downarrow
Surf.	Dist.	21.22	0.854	0.170	28.19	0.867	0.168	1.829	2.176	2.002	
	Top	18.48	0.834	0.212	27.56	0.858	0.174	2.041	2.508	2.274	
All	Dist.	20.13	0.844	0.181	27.18	0.855	0.180	2.060	2.441	2.251	
	Top	19.94	0.842	0.187	25.64	0.836	0.193	2.127	2.613	2.370	

Therefore, this paper does not cover the method for combining and utilizing uncertainties from different networks, which would be a great future work.

5.3 Analysis

We analyzed the effects of considering surface information and the distance between inputs (Algorithm 1) in image rendering and mesh reconstruction performance. In Tab. 3, the result of ActiveNeuS is shown on the first row, and it outperforms other ablations, showing that each factor has the potential to improve the rendering quality. In Blender, the selection methods that consider the distance outperform those that do not. Since camera views in Blender are distributed in a hemisphere, selecting diverse viewpoints is critical, especially in a sparse view setting. In DTU, the selection methods that consider the surface outperform others because the range of camera views is smaller than the Blender, and among the limited views, selecting views that deal with incomplete reconstruction is important. The qualitative results are shown in Appendix Sec. 7.3.

6 Conclusion

We have presented ActiveNeuS, an effective informative view selection approach that considers both geometric and image rendering fidelity. ActiveNeuS introduced a new acquisition function that efficiently and robustly utilizes a neural implicit surface uncertainty using an uncertainty grid. The acquisition function computes the integration of the neural implicit surface uncertainty by using a surface grid and applying a different integration strategy depending on the presence of the surface. We show the next-best view selection with ActiveNeuS, which improves mesh reconstruction and image rendering qualities compared to other methods. For future work, we suggest studying the effective method of joining uncertainties from different networks for informative view selection. Also, it would be interesting to apply ActiveNeuS in robotic active 3D reconstruction in which a robot arm moves and collects data.

References

1. Chen, S., Li, Y., Kwok, N.M.: Active vision in robotic systems: A survey of recent developments. *The International Journal of Robotics Research* **30**(11), 1343–1377 (2011)
2. Cover, T.M.: Elements of information theory. John Wiley & Sons (1999)
3. Delmerico, J., Isler, S., Sabzevari, R., Scaramuzza, D.: A comparison of volumetric information gain metrics for active 3d object reconstruction. *Autonomous Robots* **42**(2), 197–208 (2018)
4. Dong, W., Wang, Q., Wang, X., Zha, H.: Psdf fusion: Probabilistic signed distance function for on-the-fly 3d data fusion and scene reconstruction. In: *Proceedings of the European conference on computer vision (ECCV)*. pp. 701–717 (2018)
5. Feng, Z., Zhan, H., Chen, Z., Yan, Q., Xu, X., Cai, C., Li, B., Zhu, Q., Xu, Y.: Naruto: Neural active reconstruction from uncertain target observations. *arXiv preprint arXiv:2402.18771* (2024)
6. Gropp, A., Yariv, L., Haim, N., Atzmon, M., Lipman, Y.: Implicit geometric regularization for learning shapes. *arXiv preprint arXiv:2002.10099* (2020)
7. Isler, S., Sabzevari, R., Delmerico, J., Scaramuzza, D.: An information gain formulation for active volumetric 3d reconstruction. In: *2016 IEEE International Conference on Robotics and Automation (ICRA)*. pp. 3477–3484. IEEE (2016)
8. Jensen, R., Dahl, A., Vogiatzis, G., Tola, E., Aanæs, H.: Large scale multi-view stereopsis evaluation. In: *Proceedings of the IEEE conference on computer vision and pattern recognition*. pp. 406–413 (2014)
9. Jin, L., Chen, X., Rückin, J., Popović, M.: Neu-nbv: Next best view planning using uncertainty estimation in image-based neural rendering. In: *2023 IEEE/RSJ International Conference on Intelligent Robots and Systems (IROS)*. pp. 11305–11312 (2023). <https://doi.org/10.1109/IROS55552.2023.10342226>
10. Kajiya, J.T., Von Herzen, B.P.: Ray tracing volume densities. *ACM SIGGRAPH computer graphics* **18**(3), 165–174 (1984)
11. Kazhdan, M., Bolitho, M., Hoppe, H.: Poisson surface reconstruction. In: *Proceedings of the Fourth Eurographics Symposium on Geometry Processing*. p. 61–70. SGP '06, Eurographics Association, Goslar, DEU (2006)
12. Kendall, A., Gal, Y.: What uncertainties do we need in bayesian deep learning for computer vision? *Advances in neural information processing systems* **30** (2017)
13. Lee, S., Chen, L., Wang, J., Liniger, A., Kumar, S., Yu, F.: Uncertainty guided policy for active robotic 3d reconstruction using neural radiance fields. *IEEE Robotics and Automation Letters* **7**(4), 12070–12077 (2022). <https://doi.org/10.1109/LRA.2022.3212668>
14. Li, R., Gao, H., Tancik, M., Kanazawa, A.: Nerfacc: Efficient sampling accelerates nerfs. *arXiv preprint arXiv:2305.04966* (2023)
15. Martin-Brualla, R., Radwan, N., Sajjadi, M.S., Barron, J.T., Dosovitskiy, A., Duckworth, D.: Nerf in the wild: Neural radiance fields for unconstrained photo collections. In: *Proceedings of the IEEE/CVF Conference on Computer Vision and Pattern Recognition*. pp. 7210–7219 (2021)
16. Mildenhall, B., Srinivasan, P.P., Tancik, M., Barron, J.T., Ramamoorthi, R., Ng, R.: Nerf: Representing scenes as neural radiance fields for view synthesis. *Communications of the ACM* **65**(1), 99–106 (2021)
17. Müller, T., Evans, A., Schied, C., Keller, A.: Instant neural graphics primitives with a multiresolution hash encoding. *ACM Transactions on Graphics (ToG)* **41**(4), 1–15 (2022)
18. Pan, X., Lai, Z., Song, S., Huang, G.: Activenerf: Learning where to see with uncertainty estimation. In: *European Conference on Computer Vision*. pp. 230–246. Springer (2022)

19. Porter, T., Duff, T.: Compositing digital images. In: Proceedings of the 11th annual conference on Computer graphics and interactive techniques. pp. 253–259 (1984)
20. Ran, Y., Zeng, J., He, S., Chen, J., Li, L., Chen, Y., Lee, G., Ye, Q.: Neurar: Neural uncertainty for autonomous 3d reconstruction with implicit neural representations. *IEEE Robotics and Automation Letters* **8**(2), 1125–1132 (2023)
21. Saulnier, K., Atanarsov, N., Pappas, G.J., Kumar, V.: Information theoretic active exploration in signed distance fields. In: 2020 IEEE International Conference on Robotics and Automation (ICRA). pp. 4080–4085. IEEE (2020)
22. Thrun, S.: Probabilistic robotics. *Communications of the ACM* **45**(3), 52–57 (2002)
23. Wang, P., Liu, L., Liu, Y., Theobalt, C., Komura, T., Wang, W.: Neus: Learning neural implicit surfaces by volume rendering for multi-view reconstruction. arXiv preprint arXiv:2106.10689 (2021)
24. Yan, D., Liu, J., Quan, F., Chen, H., Fu, M.: Active implicit object reconstruction using uncertainty-guided next-best-view optimization. arXiv preprint arXiv:2303.16739 (2023)
25. Yang, J., Pavone, M., Wang, Y.: Freenerf: Improving few-shot neural rendering with free frequency regularization. In: Proceedings of the IEEE/CVF Conference on Computer Vision and Pattern Recognition. pp. 8254–8263 (2023)
26. Yu, A., Ye, V., Tancik, M., Kanazawa, A.: pixelnerf: Neural radiance fields from one or few images. In: Proceedings of the IEEE/CVF Conference on Computer Vision and Pattern Recognition. pp. 4578–4587 (2021)
27. Yu, Z., Chen, A., Antic, B., Peng, S., Bhattacharyya, A., Niemeyer, M., Tang, S., Sattler, T., Geiger, A.: Sdfstudio: A unified framework for surface reconstruction (2022), <https://github.com/autonomousvision/sdfstudio>
28. Yu, Z., Peng, S., Niemeyer, M., Sattler, T., Geiger, A.: Monosdf: Exploring monocular geometric cues for neural implicit surface reconstruction. *Advances in Neural Information Processing Systems (NeurIPS)* (2022)
29. Zhan, H., Zheng, J., Xu, Y., Reid, I., Rezatofghi, H.: Activermap: Radiance field for active mapping and planning. arXiv preprint arXiv:2211.12656 (2022)

Table 4: Comparison of the training procedures and acquisition function calculation. Both methods learn color uncertainty during training and employ the same information gain target and sampling strategy in the next-best view selection. However, the official code of ActiveNeRF [18] differs from ActiveNeRF \dagger in the sampling strategy during training.

Methods	Training		Acquisition	
	Uncert.	Sampling	Information Gain	Sampling
ActiveNeRF \dagger	true	grid	Δ color variance	hierarchy
ActiveNeRF [18]	true	hierarchy	Δ color variance	hierarchy

7 Experimental details and results

7.1 Comparison of methods

In this subsection, we elaborate on the differences in network architecture (Tab. 5) and training procedure (Tab. 4) between ActiveNeRF [18] and ActiveNeRF \dagger . In Tab. 4, ActiveNeRF [18] and ActiveNeRF \dagger differ only in the sampling strategy during training. The difference does not critically affect the final outputs’ performance, but it affects the time efficiency in training. As a result, the model with grid sampling learns faster than the model with hierarchical sampling, which can induce different next-best views sampling, leading to a better output.

For a detailed explanation, the grid sampling refers to the accelerated grid sampling utilized by NerfAcc [14] and Instant NGP [17]. The grid sampling method selects 3D points by referencing an occupancy grid. During ray marching, the sample point within an occupancy grid cell with a lower occupancy probability than a given threshold is skipped. Therefore, with grid sampling, a variable number of samples are chosen in each ray. We employed grid sampling for efficient and rapid training.

On the other hand, the hierarchical sampling [16] samples a constant N points using a coarse network and a fine network ($N = N_c + N_f$). The coarse network first samples N_c points and evaluates the points to provide density information to the fine network. The fine network considers N_f points’ importance for final volume rendering results during sampling. Hierarchical sampling operates with a similar intention to grid sampling, but it is inefficient in that it has to sample N points even if the camera ray traverses a vacant space. We used the hierarchical sampling for the acquisition value in ActiveNeRF \dagger because, in Eq. (11), constant N samples need to be sampled in a ray.

In Tab. 5, we used the NeuS [23] architecture for models with SDF representation and the NeRF [16] architecture for networks with density representation. Except for ActiveNeRF [18], all networks are implemented based on SDFstudio [27]. Regarding hyper-parameters, we adjusted the loss coefficients of our architectures as we could not reproduce the results with the official code of ActiveNeRF [18]. The original uncertainty loss coefficient penalized the density so hard that sampling 3D points with grid sampling easily failed as the grid sampling samples a varying number of points. Consequently, we reduced the uncertainty loss coefficients to infer color uncertainty while maintaining high rendering performance.

Table 5: Details in network architectures of ActiveNeRF[†] (in surface and density representation) and ActiveNeRF [18].

Networks		Surface	Density	ActiveNeRF [18]
Density or SDF network	MLP hidden layer	8	8	8
	MLP size	256	256	256
	Activation	Softplus	ReLU	ReLU
	positional encoding	6	10	10
	skip connection layer	4	4	4
Color network	MLP hidden layer	4	1	1
	MLP size	256	128	128
	direction encoding	4	4	4
Hyper-parameters	RGB loss	1	1	1
	eikonal loss	0.1	-	-
	uncertain loss (RGB)	0.001	0.001	1
	uncertain loss (beta)	0.01	0.01	0.5
	uncertain loss (sigma)	0.0	0.0	0.01
	beta min	0.001	0.001	0.01
	Batch size	512	512	1024
	Learning rate	5×10^{-4}	5×10^{-4}	5×10^{-4}

7.2 Experiment settings

In this subsection, we provide detailed explanations about the active learning scheme, including the number of total iterations, selection intervals, the number of steps for frequency regularization, and the duration of the warm-up stage. The total training iterations in the Blender dataset’s 1, 2, and 4-image settings are $50k$, $100k$, and $200k$, respectively. For the DTU dataset, we trained models for $60k$ iterations in the 2-image setting and $120k$ iterations in the 4-image setting. In terms of selection intervals, in the 2-image setting, the model selects the next-best views (NBV) for every $1k$ iteration (e.g., $[1k, 2k, 3k, 4k]$), and in the 4-image setting, NBV selection occurs every $2k$ iteration (e.g., $[2k, 4k, 6k, 8k]$). Similarly, the model selects the NBV for every $0.5k$ iteration in the 1-image setting, (e.g. $[0.5k, 1k, 1.5k, 2k]$). As the model selects NBVs four times, the total numbers of train images are 5, 10, and 20 in 1, 2, and 4-image settings, respectively.

We applied frequency regularization in the 1-and 2-image settings, as suggested in FreeNeRF [25]. Given the challenge of learning from a few images and inferring the next-best view, frequency regularization helped the model choose useful images by initially evaluating them with low frequency and gradually transitioning to high frequency. Following a setup similar to FreeNeRF [25], the frequency regularization ends at $40k$ iterations (40% of total iterations) when the model is trained on 2-image setting Blender, $30k$ iterations (60% of total iterations) on 1-image setting Blender, and at $30k$ iterations (50% of total iterations) for models trained on 2-image setting DTU.

We used two warm-up stages, one from the NeuS [23] framework and the other from sampling strategies. According to NeuS [23], training a model to converge and learn a surface is challenging, so setting the learning rate of surface representation networks to linearly warm up helps training. Therefore, we implemented the NeuS networks’ learning rate to increase from 0 to 5×10^{-4} in the first 500 iterations in the 1 and 2-image settings and 1000 iterations in the 4-image setting.

During the warm-up stage in sampling strategies, hierarchical sampling is used instead of grid sampling to sample from various locations in the scene. Additionally, all cells in the occupancy grid are updated. After the warm-up stage, 3D points are sampled with grid sampling, and the occupancy grid is partially updated by selecting n_o occupied cells and n_r randomly sampled cells, where n_o and n_r are parameters. It is important to note that the warm-up stage is lengthened if the model is trained on more images in different settings.

7.3 More results

We report additional qualitative results of NBV selection in the 2- and 4-image settings on the Blender and the DTU dataset. Our image rendering and mesh reconstruction show clearer results in Fig. 7a, and similar to the mesh reconstruction results shown in Fig. 4c, density-Random may output reasonably rendered images. Still, the resulting mesh is unrecognizable (Fig. 7b). Also, in the DTU dataset, our method infers more detailed meshes than surface-Random and density-ActiveNeRF† fails to recover accurate meshes without explicit surface inference.

We also report qualitative results in ablation studies (Fig. 10, Fig. 9). In Fig. 10, the chair exhibits bulky noise between the armrests in Surf. + Top-K. This type of error frequently occurs when the camera views are inadequately chosen. Also, spreading out the camera views is important, especially when reconstructing objects with light reflections, as shown in Blender materials. In Fig. 9, we demonstrate that selecting camera views by referencing the surface information leads to diverse camera selection across scenes. As the DTU dataset has a smaller range of camera views than Blender, cases labeled ‘All’ have similar views across scenes, while cases labeled ‘Surface’ exhibit diverse selections.

We provide additional rendering results in various viewpoints by ActiveNeuS in the 2-image setting on DTU (Fig. 8). Also, we present more results in the 2-image setting on Blender in Fig. 11. ‘mic’ in Blender is a challenging scene, so rendering ‘mic’ with inadequately chosen images frequently results in blank rendered images. ActiveNeRF† could not converge the ‘mic’ image with the chosen camera views under the same hyperparameter setting as for other scenes.

7.4 Multiple next-best view selection

Algorithm 1 outlines selecting multiple next-best views that cover a wider range of XYZ coordinates. The main idea is to select views with high acquisition value while considering the distance from the already incorporated train views. A view is selected if it has a longer distance than the distance threshold τ from all train views and has the highest acquisition value among the satisfied candidates. We empirically set τ to

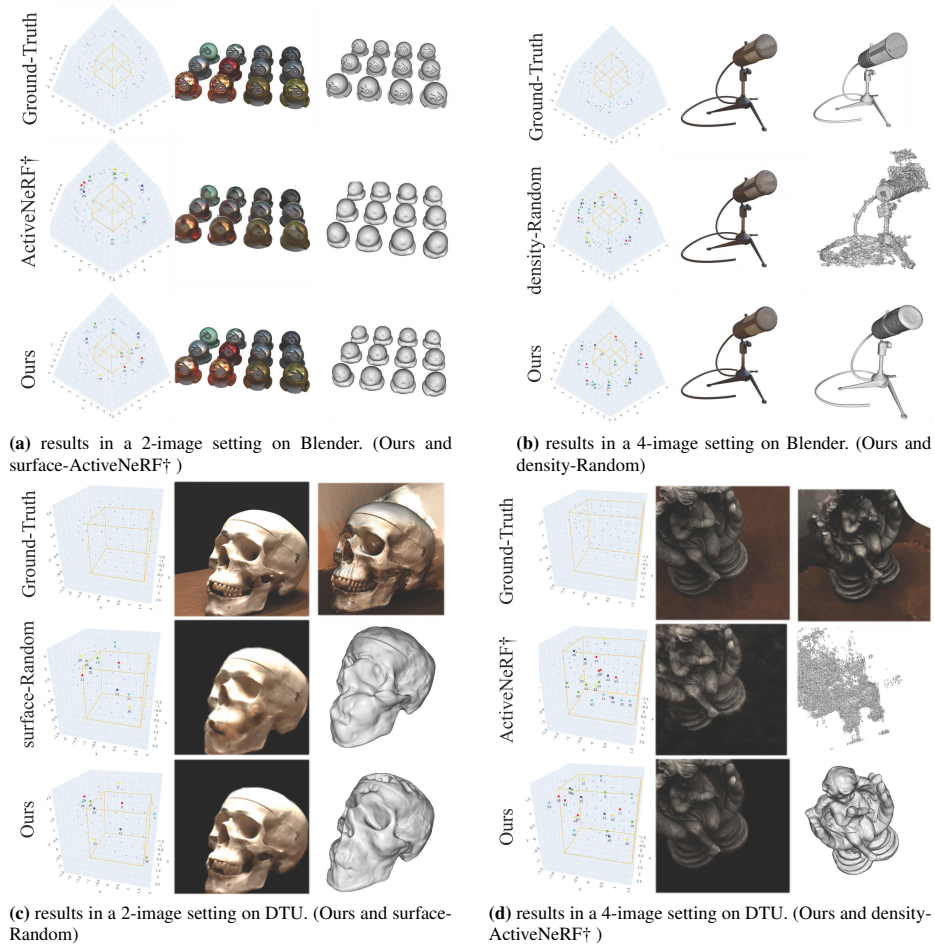


Fig. 7: Ground-Truth and the best-performing algorithms are compared. The visualization of camera coordinates of selected train images, rendered RGB images, and reconstructed meshes are shown from left to right. The camera inputs are chosen in the order of blue-cyan-green-yellow-red. Since object scenes have different total numbers of train images, different camera poses are selected even though we fixed the random seed. Also, in DTU, 10 test images are excluded from the training set from the start, but they are still shown on the camera poses visualization of Ground-Truth. The mesh reconstruction of the DTU dataset, composed of point clouds, was performed using Kadzhdan *et al.* [11]. We use the same Chamfer distances evaluation used in MonoSDF [28].

1.732, and when no candidate satisfies the distance threshold, the threshold decreases by multiplying it with the decay factor 0.95.

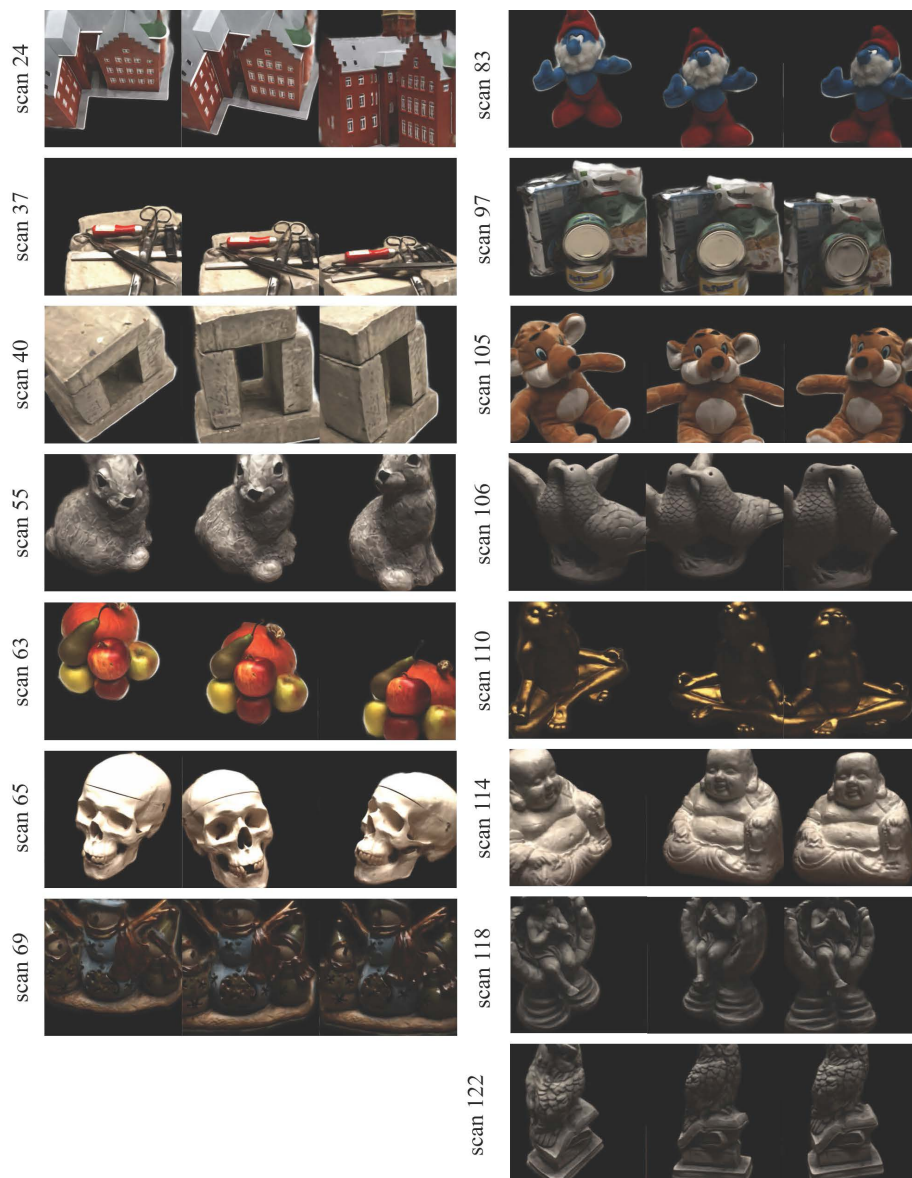


Fig. 8: Qualitative results of ActiveNeuS in a 2-image setting on DTU.

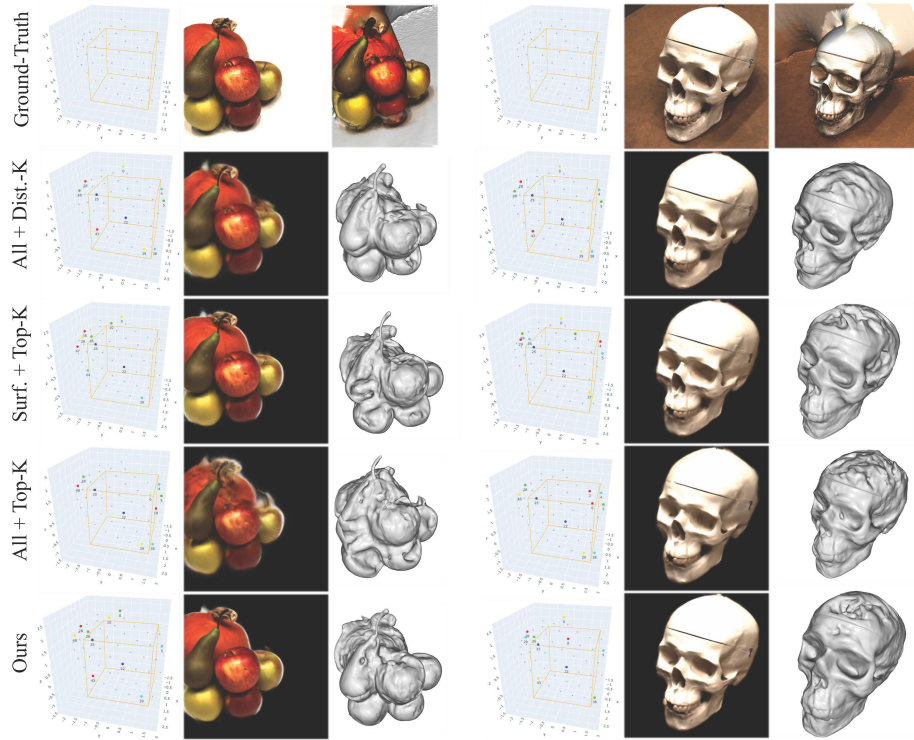


Fig. 9: Qualitative results in ablation studies on DTU. The visualization of camera coordinates of selected train images, rendered RGB images, and reconstructed meshes are shown from left to right. The camera inputs are chosen in the order of blue-cyan-green-yellow-red. The Ground-Truth mesh reconstruction of the DTU dataset, composed of point clouds, was performed using [11].

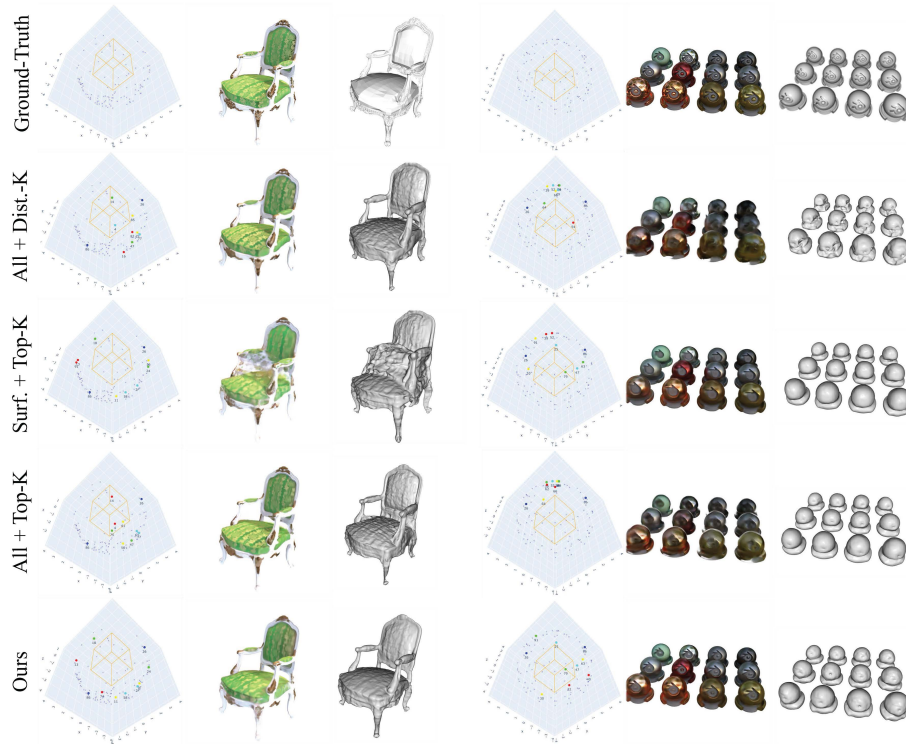


Fig. 10: Qualitative results in ablation studies on Blender. The visualization of camera coordinates of selected train images, rendered RGB images, and reconstructed meshes are shown from left to right. The camera inputs are chosen in the order of blue-cyan-green-yellow-red. Given that the Blender training set's cameras are positioned on a hemisphere, we tilted the 3D coordinates for a clearer comparison. Our selection of camera views covers wider views, including top and 360-degree views, resulting in more accurate rendering and meshes.

Algorithm 1 Multiple next-best view selection

-
- 1: **Input:** candidate camera index array C , train camera index array T , camera pose array P , acquisition function G_s , distance threshold τ , the number to select K
 - 2: **Output:** next-best view index array A
 - 3: select idx from C that has the maximum G_s value
 - 4: remove idx from C and add idx in A
 - 5: **for** $i \leftarrow 1$ to $K - 1$ **do**
 - 6: add idx in T and descending sort C by the G_s value
 - 7: compute the pairwise distance matrix D between $P[T]$ and $P[C]$
 - 8: get a boolean matrix $B_C = (D \geq \tau)$ and do "AND" operation along T
 - 9: **while** B_C is all False along C **do**
 - 10: $\tau \leftarrow \tau \times 0.95$ ▷ Lower the distance threshold
 - 11: $B_C = (D \geq \tau)$ and do "AND" operation along T ▷ Filter again with the relaxed criteria
 - 12: $idx = C[B_C][0]$ ▷ Select the first element in sorted C filtered with the distance
 - 13: remove idx from C and add idx in A
-

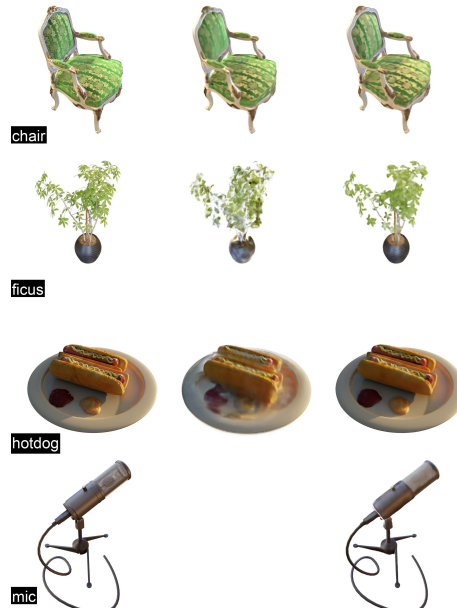


Fig. 11: Qualitative results of Ground Truth, surface-ActiveNeRF†, and ActiveNeuS in a 2-image setting on Blender.